Cage Molecules Stabilize Lead-halide Perovskite Thin Films

Shijing Sun[1*†], Ming Liu[2*‡], Janak Thapa[1], Noor Titan Putri Hartono[1§], Yicheng Zhao[3,3a], Donglin He[2], Sarah Wieghold[4], Matthew Chua[1], Yue Wu[2], Vladimir Bulović[1], Sanliang Ling[5], Christoph J. Brabec[3,3a], Andrew I. Cooper[2*], Tonio Buonassisi[1*]

[1]Massachusetts Institute of Technology, Cambridge, MA USA 02139

[2]Materials Innovation Factory, University of Liverpool, Liverpool UK L7 3NY

[3]Helmholtz Institute Erlangen-Nürnberg for Renewable Energy, Erlangen, Germany 91058

[3a]Institute of Materials for Electronics and Energy Technology (i-MEET), FAU, Erlangen, Germany 91058

[4]Argonne National Laboratory, Lemont, IL USA 60439

[5]Advanced Materials Research Group, Faculty of Engineering, University of Nottingham, Nottingham NG7 2RD, U.K.

ABSTRACT: The environmental stability of hybrid organic-inorganic perovskite (HOIP) materials needs to increase, to enable their widespread adoption in thin-film solar and optoelectronic devices. Molecular additives emerged recently as an effective strategy to regulate HOIP crystal growth and to passivate defects. However, to date the choice of additives is largely limited to a dozen or so materials under the design philosophy that high crystallinity is a prerequisite for stable HOIP thin films. In this study, we incorporate porous organic cages (POCs) as functional additives into perovskite thin films for the first time and investigate the HOIP-POC interaction via a combined experimental and computational approach. POCs are significantly larger than small molecule additives explored for HOIP synthesis to date but much smaller than polymeric sealants. Partially amorphized composites of $MAPbI_3$ (methylammonium lead iodide, HOIP) and RCC3 (an amine POC) form a network-like surface topography and lead to an increase in the optical bandgap from 1.60 eV to 1.63 eV. Further *in situ* optical imaging suggests that RCC3 can delay the $MAPbI_3$ film degradation onset up to 50 × under heat and humidity stresses, showing premises in reliability improvement for HOIP-based solar-cell and light-emitting applications. Furthermore, there is evidence of molecular interactions between RCC3 and $MAPbI_3$, as fingerprinted by the suppressed N-H stretching mode in MA^+ from Fourier transform infrared spectroscopy (FTIR) and by density functional theory (DFT) simulations, which suggest strong hydrogen bonding between MA^+ and RCC3. Given the diversity of POCs and HOIPs, our work opens a new avenue to stabilize HOIPs via tailored molecular interactions with functional organic materials.

Despite the outstanding optoelectronic properties of HOIPs, prototypical halide perovskites, such as methylammonium lead iodide ($MAPbI_3$, MA = CH_3NH_3), suffer from their poor environmental stability.[1] The rapid degradation of the photoactive $MAPbI_3$ phase in the presence of heat, light, oxygen, or moisture is attributed to both chemical and structural instability, arising from the volatility of organic components, defect-induced ion migration within the inorganic frameworks, and phase transitions.[2] At a microscopic level, there has been intensive research in additive engineering to modify the crystallization kinetics of lead-halide perovskites, yielding high-quality polycrystalline thin films.[3,4] While the benefits of additives were first demonstrated through improved solar-cell efficiency,[5,6] new additives are increasingly sought to engineer device reliability.[7] For example, small molecules such as 5-aminovaleric acid (molecular weight, MW, of 117.15 g/mol) and adipic acid (MW of 146.14 g/mol) proved effective in improving solar cells and light-emitting diodes (LEDs) operational stability via interface passivation.[4,8]

While a wide range of additives has been considered recently to modify perovskite stability, including salts, small molecules, polymers, and nanoparticles, molecular additives are particularly attractive because of their compatibility with the low-cost solution process.[9–11] State-of-the-art molecular additives typically improve perovskite thin-film stability through two strategies. The first strategy is indirect influence, whereby modification of the nucleation and growth kinetics give rise to polycrystalline perovskites containing larger grains, fewer grain boundary defects, and higher crystallinity.[10,12] Such defect management blocks the pathways for water and oxygen molecules to migrate into the perovskite structure, enabling $MAPbI_3$ films to be more resistant to environmental stresses. The second strategy is direct influence: recent advances in molecular engineering have introduced functional additives that remain chemically active in perovskite films after synthesis, either by becoming part of the perovskite crystal structure or by precipitating at the grain boundaries.[13] Small amine cations such as butylammonium (BA) and phenethylammonium (PEA)

are readily incorporated into the perovskite lattice, forming more temperature- and moisture-stable two-dimensional (2D) perovskites.[14] Large polymeric additives such as poly(ethyl 2-cyanoacrylate), on the other hand, improve the perovskite film stability by sealing the grain boundaries and passivating the surface with their hydrophobic functional groups.[9]

In the abovementioned state-of-the-art approaches, HOIP stability is enhanced by engineering the crystalline domains of perovskite films. This is motivated by the understanding that a single perovskite crystal with no defects would be stable.[15,16] Common additive incorporations, therefore, are based on the rationale that perovskite environmental stability requires improved crystallinity and defect passivation in polycrystalline films.[17] In this study, we report a third approach by introducing a new type of molecular additive, porous organic cages (POCs), that promotes disorder instead of ordered grain growth yet still enables significant moisture and thermal stability improvement for $MAPbI_3$ thin films. We report a mechanistic study of unique POC-HOIP molecular interactions through hydrogen bonding and demonstrate a resultant reliability enhancement at the device level. Our combined experimental and computational studies on perovskite phase stabilization by POCs open a new pathway to structurally engineer the previously under-explored amorphous domains of functional HOIP thin films.

POCs are an emerging subclass of molecular materials that comprise discrete cage molecules. Unlike their extended framework material counterparts, such as metal-organic frameworks (MOFs) and covalent organic frameworks (COFs), most POCs are solution processable. They have been explored for applications in gas storage, organic molecule separation, and as catalyst supports.[18–20] POCs show distinct features that are different from the existing molecular additives employed in the HOIP field: typical POC molecules are large (MW > 1000 g/mol), bulky (> 5 Å in all three dimensions), and POC crystals are generally microporous (surface area > 300 $m^2\ g^{-1}$).[21] They can also contain multiple functional groups in a single molecule. In this study, we focus on RCC3, an amine POC that contains 12 symmetrically placed amine groups within its molecular cavity. We selected RCC3 to investigate the effect of cage molecules on HOIP in this study for three reasons. Firstly, RCC3, and its parental imine cage CC3, are the most representative and well-studied porous organic cages (POCs) in the field.[22] The results on RCC3 will guide us to select other amine cages, optimize the structure of cages, and synthesize new cages in the future for the same application. Secondly, HOIP degradation due to interactions between the volatile MA+ and water and oxygen is a significant challenge in commercializing MA-based HOIP materials for clean energy applications. In this study, we design experiments to test the functionality of cage molecules to interact with MA+. We therefore picked RCC3 which has a suitable cavity to accommodate MA^+. Thirdly, RCC3 is readily soluble in most organic solvents, including common solvents used to fabricate lead-halide perovskites, such as dimethylformamide and dimethyl sulfoxide (Table S1). It has also been proven scalable in synthesis in our previous study, which could be very crucial for commercialization in the future.[21] Figure 1a demonstrates the synthetic workflow for incorporating RCC3 powder into the perovskite precursor solution, followed by a one-step spin-coating process and annealing to facilitate $MAPbI_3$ grain crystallization.

The addition of RCC3 was found to increase the perovskite phase stability significantly. Figures 1b-c indicate that after seven days under ambient conditions (October, MA, USA), the reference $MAPbI_3$ films underwent severe degradation, leading to the emergence of the inorganic decomposition product, PbI_2. In contrast, no PbI_2 was observed in RCC3-$MAPbI_3$ (37 ± 3 mM of RCC3; referred to in this study as 37 mM; the standard deviation accounts for solubility variation upon storage). The crystalline $MAPbI_3$ phase in this composite remained intact at the end of the 7-day testing. Interestingly, the powder X-ray diffraction patterns of POC-HOIP composites exhibit distinctive features that are different from the two known perovskite stabilization mechanisms *via* compositional engineering: 1) there is an absence of new crystalline phases, which excludes the formation of more stable 2D Ruddlesden–Popper perovskites, a mechanism that often results from the addition of smaller amines;[23] and 2) instead of promoting ordered grain growth as expected for common molecular additives and polymer scaffolds, Comparing the crystallinity of $MAPbI_3$ in Figure 1b and RCC3-$MAPbI_3$ in Figure 1c, RCC3 is found to reduce crystallinity.

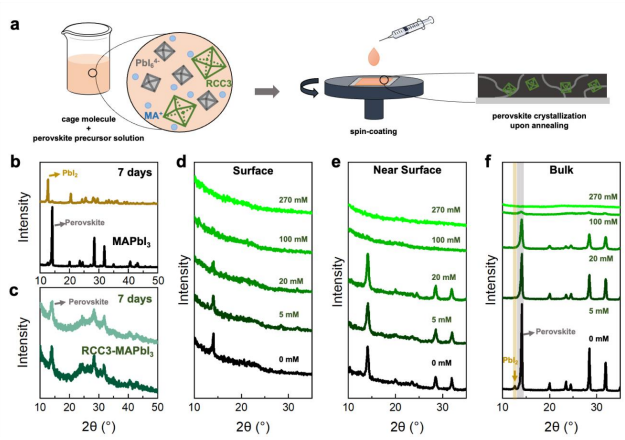

Figure 1(a) Solution synthesis workflow for POC-HOIP thin films. Grazing-incidence X-ray diffraction (GIXRD) patterns are shown for (b) as-synthesized and after-7-days $MAPbI_3$ and (c) as-synthesized and after-7-days RCC3-$MAPbI_3$ (37 ± 3 mM RCC3 in precursor solution). RCC3-$MAPbI_3$ films were examined with GIXRD incident angles of (d) 0.08°, (e) 0.2°, and (f) 1° to probe the crystal structure of films at various penetration depths.

To better understand the precipitation of RCC3 within $MAPbI_3$ films, we compared the crystal structures of $MAPbI_3$ films with varying RCC3 concentrations (5, 20, 100, and 270 mM). The results show that the $MAPbI_3$ film becomes partially amorphous with increased RCC3 loadings. Grazing-incidence X-ray diffraction (GIXRD) with an incident angle of 0.08° was used to probe the $MAPbI_3$ structure at the film surface. Figure 1d shows that the intensity of the $MAPbI_3$ reflection at 14.5° gradually decreases with increasing RCC3 concentration. To further explore the distribution of amorphous perovskites underneath the film surface, we compared the crystal structure at different depths by varying the incident angle of the GIXRD measurements from 0.08° to 1°. The results show that POC-HOIP composites do not sit only at the surface of perovskite films but distribute inside the bulk film, unlike in previous reports where stabilization could be achieved by depositing an amorphous capping layer atop the perovskites.[24] Furthermore, while a small amount of PbI_2 was present in $MAPbI_3$, because that over-stoichiometric PbI_2 addition was used in our standard synthesis protocol,[25] PbI_2 was not visible in as-synthesized RCC3-$MAPbI_3$. The crystallization of excess PbI_2 was likely suppressed by the interactions between RCC3, PbI_2, and DMF/DMSO solvents prior to perovskite growth. The as-synthesized films with 100 mM or less RCC3 remain black like the pristine $MAPbI_3$. In contrast, films made with 270 mM RCC3 were dark yellow, indicating significant suppression in perovskite crystallization with excess RCC3.

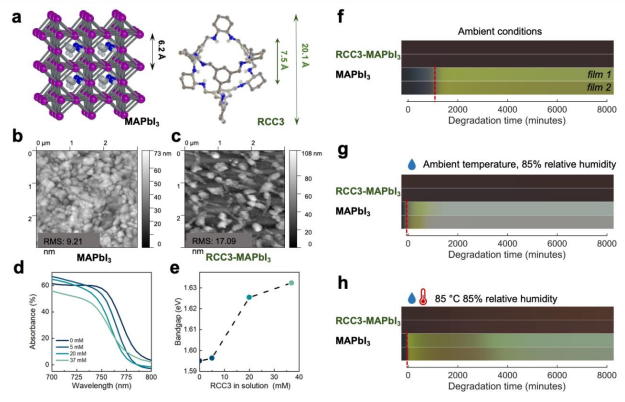

Figure 2 (a) Crystal structures of $MAPbI_3$ and RCC3. Carbon and nitrogen atoms are shown in grey and blue, respectively. Hydrogen atoms in RCC3 are omitted for clarity, except in the secondary amine group of RCC3. Atomic force microscopy (AFM) images are presented for (b) $MAPbI_3$ and (c) RCC3-$MAPbI_3$ (37 ± 3 mM RCC3 in precursor solution). RMS units are in nm. (d) Absorption edges of RCC3-$MAPbI_3$ films measured by UV-visible spectroscopy and (e) optical bandgaps of RCC3-$MAPbI_3$ estimated by the Tauc method (estimated standard deviation of 2%) as a function of POC concentration in the precursor solution.[26] (f)-(h) *In situ* optical imaging of perovskite thin-film degradation under ambient conditions (October, MA, USA), 85% relative humidity (RH) at ambient temperature, and 85% RH at 85 °C, respectively (all with 0.15 Sun illumination for imaging). For each composition, two as-synthesized films of (1 × 0.5) in^2 were degraded side-by-side for repeatability purposes. RCC3 – 37 mM - $MAPbI_3$ was used for all the *in situ* film degradation tests.

To date, few studies investigated perovskite amorphization via additive engineering. Garnett *et al.*[27] reported the synthesis of partially amorphized $MAPbI_3$ film by adding methylammonium acetate (MW of 91 g/mol), where first-principle calculations suggested that the small acetate ions interact with perovskite at an atomic scale and partially replace iodide in the perovskite lattice. On the other hand, organic polymers, e.g., polyethylene glycol (PEG, MW ~20k g/mol), are reported to modify microscale film morphology and enhance crystallinity through templated grain growth.[28–30] POCs crystalize in the form of discrete molecules and exhibit a molecular weight of ~ 1k g/mol,[31] are therefore expected to favor interaction mechanisms with HOIPs, that are different from the much larger polymer additives or the much smaller organic molecules. Figure 2a compares the relative sizes, shapes, and crystal structures of RCC3 and $MAPbI_3$. An individual porous RCC3 molecule exhibits an inner cavity diameter of 7.5 Å and an outer diameter of 20.1 Å, whereas cubic $MAPbI_3$ show a lattice parameter (I – I distance) of 6.2 Å, around one-third the size of an RCC3 molecule. In Figures 2b-c, atomic force microscopy (AFM) was employed to probe the surface topography of the perovskite and POC-HOIP films, respectively. A network-type microstructure was visible at the surface of the otherwise homogeneous polycrystalline thin films upon RCC3 addition (Figure S1), leading to an increase in film roughness from a root mean square (RMS) value of 9.2 nm in $MAPbI_3$ film to 17.1 nm in RCC3-$MAPbI_3$ (37 mM). Surface contact potential measurements using Kelvin probe force microscopy (KPFM) further show that the RCC3 leads to surface potential changes, suggesting a slight modification of the work function at the interface depending on the RCC3 concentration (Figure S2). From UV-visible spectroscopy measurements, we observed a blue shift of the absorption edge in the partially amorphous films, which led to an increased bandgap from 1.60 eV (0 mM) to 1.63 eV (37 mM) (see Figure 2d-e). The POC-induced bandgap increases might be led by octahedral tilting within the perovskite framework[32] following an increasing degree of amorphization.

To quantify the influence of RCC3 on perovskites' environmental stability, we performed comparative aging experiments using *in situ* optical imaging to monitor the degradation behavior of $MAPbI_3$ and RCC3-$MAPbI_3$ (37 mM) synthesized using the same batch of perovskite precursors. Figures 2f-h indicate that RCC3-$MAPbI_3$ can stabilize the dark-colored photoactive phase under ambient, humid, and hot-humid conditions. These results suggest that RCC3 hinders the moisture-induced and heat-induced degradation of polycrystalline $MAPbI_3$ films, both of which are significant obstacles to commercializing MA-containing perovskites for clean energy applications.[33] The dark-colored reference $MAPbI_3$ film rapidly decomposes under elevated humidity to yellow PbI_2, followed by a more transparent hydrated lead iodide complex, consistent with our previous studies and literature reports.[34,35] Zooming into the first 2000 minutes of the aging tests, we quantify the degradation onsets of reference $MAPbI_3$ through the optical changes recorded by red, green, and blue (RGB) channels (Figure S3 and Table S2). In best-performing films of RCC3-$MAPbI_3$, a consistent dark color was maintained for over 8000 minutes under elevated temperature (85°C) and humidity (85% RH) conditions, indicating a 50× delay of degradation onset relative to $MAPbI_3$ controls (160 minutes), using an RGB camera (Table S1). However, we should note that this result did vary during our verification experiments under high humidity, making it challenging to quantify the optimal concentrations of RCC3 to stabilize perovskite films (Figure S4). The stabilization effect was observed to drop with increased RCC3 storage time in a glovebox, perhaps due to POCs capturing gas molecules or adventitious water over time.[22] While the stability performances of individual samples were consistent within a batch, as seen in Figure 2f-h, there were batch-to-batch variations in the reference $MAPbI_3$ degradation onsets over months, likely due to the changing $MAPbI_3$ solution synthesis baselines (Figure S4). Efforts to reproduce and expand upon these results should pay extra attention to process control, both for the HOIP film and POC additive. Nevertheless, under the *in situ* testing conditions applied in this study, the POC additive method shows the potential to overperform state-of-the-art composition engineering method forming MA, formamidinium (FA) and caesium mixed-cation perovskites (17 × stability improvement relative to $MAPbI_3$)[34] and the capping method using phenyltriethylammonium (PTEA) iodide forming 2D/3D heterostructured perovskites 4 - 6 × stability improvement relative to $MAPbI_3$) as reported in our previous studies.[36,37] Additional stability tests for a list of small molecular additives and other POCs, including RCC1, RCC1-HBr, and RCC1-HBr at solar cell-relevant low concentrations are shown in Figure S5–7. We believe that the enormous structural, chemical and geometrical diversity of the POC family provides a rich platform for designing and optimizing additives to stabilize perovskite thin films in the future. Moreover, these molecules occupy an interesting regime in molecular size, being significantly larger than small molecule additives but much smaller than polymeric sealants.

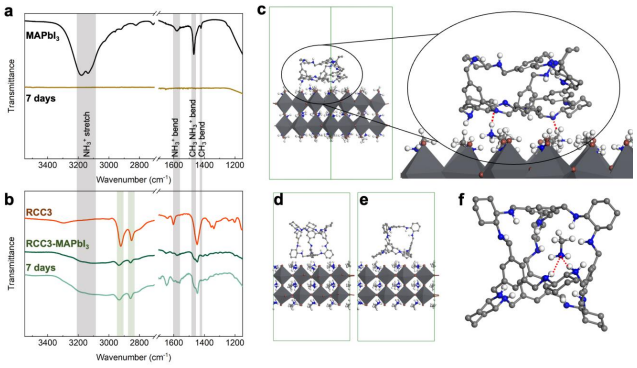

Figure 3 (a) Attenuated total reflection-Fourier transform infrared spectroscopy (ATR-FTIR) measurements for as-synthesized $MAPbI_3$ films and $MAPbI_3$ stored for seven days in ambient conditions (October, MA, USA). (b) ATR-FTIR spectra for as-synthesized RCC3 powder, as-synthesized RCC3-$MAPbI_3$ (37 ± 3 mM RCC3 in precursor solution) and RCC3-$MAPbI_3$ stored for seven days in ambient conditions same as 3 (a). As references, key features of an as-synthesized $MAPbI_3$ thin film and RCC3 powder are highlighted in grey and green. (c) DFT optimized structure of nonporous RCC3 on $MAPbI_3$ (001) surface, with initial structure taken from the AIMD trajectory. Red dotted lines indicate hydrogen bonds. Hydrogen atoms in RCC3 (except those bonded to N) are omitted for clarity. (d)-(e) DFT optimized structures of $MAPbI_3$/RCC3 interface with two different configurations: (d) config-1, benzene facet of RCC3 on $MAPbI_3$ and (e) config-2, hollow facet on $MAPbI_3$. (f) MA^+ in RCC3 with intermolecular proton transfer. Red dotted lines indicate hydrogen bonds. Hydrogen atoms in RCC3 (except those bonded to N) are omitted for clarity. Colour code: H - white, C - light grey, N - blue, O - red, Pb - dark grey, I - brown.

To better understand the origin of structural stabilization in $MAPbI_3$-RCC3, we examined the molecular interactions between the POC and the HOIP via combined experimental and computational approaches. Attenuated total reflection-Fourier transform infrared (ATR-FTIR) spectroscopy revealed that without RCC3, no chemical bonds from the organics were detected at the surface of the thin-film $MAPbI_3$ after being stored in ambient conditions for seven days (October 2020, MA,

USA). As shown in Figure 3a, the flat transmission curve across 1000 cm^{-1} to 4000 cm^{-1} in the degraded $MAPbI_3$ sample indicates a complete escape of the volatile MA^+ from the inorganic perovskite framework. In contrast, Figure 3b shows that signals of MA^+ and organics in RCC3 remain unchanged in the RCC3-$MAPbI_3$ (37 mM) film after the 7-day testing, confirming a stabilized organic-inorganic network in the POC-HOIP system in comparison to the bare polycrystalline perovskite films. From the FTIR measurements, the fingerprint region of RCC3 (highlighted in green) and the MA ions (highlighted grey) are both observed in the as-synthesized RCC3-$MAPbI_3$ (dark green), which is evidence that RCC3 precipitates and remains in the $MAPbI_3$ films after synthesis. Figure S8 indicates that with as low as 5 mM of RCC3 addition, RCC3 signals arising from the C-H stretching of cyclohexane groups (2950 cm^{-1} and 2850 cm^{-1}) and C-C stretching of benzyl rings (1600 cm^{-1} and 1450 cm^{-1}) were detected in RCC3-$MAPbI_3$. Interestingly, despite preserving the N-H bend and C-N bend modes in MA^+, the N-H stretch mode of MA^+ within $MAPbI_3$ was significantly suppressed and broadened in the presence of RCC3. This suggests that RCC3 is not only physically present in perovskite films but remains chemically active through hydrogen bonding with MA^+.

To investigate the nature of interactions between RCC3 and $MAPbI_3$ at the atomic scale, we performed *ab initio* molecular dynamics (AIMD) simulations at 400 K, considering an isolated porous RCC3 cage molecule sitting on top of the $MAPbI_3$ (001) surface (Video S1). The results show that RCC3 collapses to its amorphous and non-porous form after ten ps, consistent with the fact that RCC3 does not exhibit permanent porosity in the solid state. As seen in Figure 3c, as the cage molecule collapses, the cyclohexyl vertex groups of RCC3 move away from $MAPbI_3$ slightly, which enables the -NH- moiety in RCC3 to move closer towards the $MAPbI_3$ (001) surface. Such dynamics facilitate the formation of strong hydrogen bonds between MA^+ from $MAPbI_3$ and the -NH- moiety from RCC3 (see an enlarged demonstration in Figure 3c), which is consistent with the experimental observation from FTIR of RCC3-$MAPbI_3$ with as low as 5 mM of RCC3 addition (Figure S8). We therefore propose a possible protective mechanism that RCC3 impedes the volatile MA^+ from escaping the perovskite surface by forming hydrogen bonds; at the same time, the collapsed amorphous RCC3 network acts like a sticky cover on $MAPbI_3$ and suppresses the motion of MA^+. While there could be some interactions between I- anions and hydrogens in RCC3, MA+ forms a strong hydrogen bond with the -NH- moiety of RCC3 (where N is the H-bond acceptor, see an enlarged demonstration in Figure 3c). Due to the large size of RCC3, there is no direct competition between these two types of interactions, as I^- and MA^+ interact with different parts of the RCC3 molecule. In our discussions, we focus on the interactions between RCC3 and MA+, as it is known that MA^+ dissolution is one of the dominant mechanisms leading to the degradation of MAPbI3 under high humidity.[38,39]

Previous studies show that POCs can "open up" and transform into a porous form to accommodate guest molecules such as SO_2 and H_2O.[21,40] To explore the possibility of MA^+ migration into the porous RCC3, we calculated the energy at the interface of $MAPbI_3$ and porous RCC3. Figures 3d and 3e demonstrate two possible porous RCC3 configurations, where the $MAPbI_3$(001) surface interfaces with the benzene and hollow facets of RCC3, respectively. Density functional theory calculations (DFT) show that these two configurations exhibit similar energies. The interaction is likely weak due to steric repulsion between $MAPbI_3$ and cyclohexyl vertex groups in RCC3 (see Figure S9 for two perovskite configurations considered). We then re-optimized the RCC3 structure with MA^+ inside the RCC3 cavity. The results revealed that it is energetically favorable for MA^+ to sit inside RCC3, owing to the formation of a strong hydrogen bond between MA^+ and -NH- moiety of RCC3. Further AIMD simulation at 400 K reveals that MA^+ would be released from the cage molecule at the same time when RCC3 collapses to its non-porous form (Video S2). These first-principles calculations suggest that $MAPbI_3$ could be stabilized through MA^+ forming hydrogen bonding from inside of the cage (see Supporting Information for computational methods). Since it is energetically favorable to form hydrogen bonds in both the scenarios when the MA+ is outside of the cage (RCC3 in a collapsed form) and when MA+ is inside of the cage (RCC3 in an open form, with MA^+ trapped), the attachment MA^+ onto the nearby cage molecules shows an effective protective mechanism against MA^+ loss from the HOIP. The simulation results are consistent with the observed delayed macroscale thin-film degradation (Figure S10).

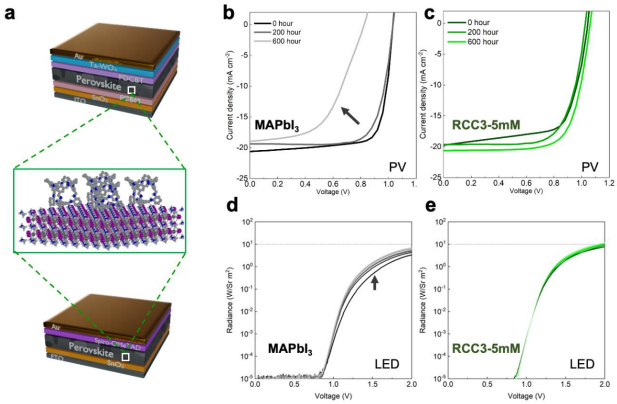

Figure 4 (a) Device architecture of solar cells and LEDs fabricated in this study. Note: for solar cell reliability tests, PCBM was removed to improve the interfacial stability at the ETL/perovskite interface in ambient air. The locations shown for the cage molecules are for illustration purposes only and are not meant to indicate precise lattice locations. (b)-(c) Operation stability of solar devices based on $MAPbI_3$ and RCC3-5 mM-$MAPbI_3$, respectively. (d)-(e) Illumination of light-emitting devices based on $MAPbI_3$ and RCC3-5 mM-$MAPbI_3$ as a function of voltage sweeps.

We further tested the potential of RCC3-$MAPbI_3$ for optoelectronic applications employing the POC-HOIP composite for the first time as active layers in solar and light-emitting devices (Figure 4a). Photovoltaic performances (PV) measurements show that the materials-level stabilization led by RCC3 is transferrable to solar device reliability. To minimize degradation at the ETL/perovskite interface in ambient air, for the long-term solar cell aging test, the device structure is changed from SnO_2-nanoparticle/PCBM/Perovskite/PDCBT/Ta-WOx/Au (Figure 4a, Figure S12) to SnO_2-nanoparticle/Perovskite/PDCBT/Ta-WOx/Au. Figures 4b-c show that the RCC3-$MAPbI_3$ (5 mM) solar cell shows negligible efficiency loss after 600 hours of aging at 80 °C in ambient air with 30–50% RH (16% of PCE efficiency). The stability improvement is mainly attributed to the protective effect of RCC3 in suppressing the interactions between perovskite and water/oxygen during the aging period, which is consistent with the film stability tests showing reduced MA^+ diffusion. Figures 4d-e indicate that when driven from extended (>2h) rest in the dark, the RCC3-$MAPbI_3$ (5 mM) LED exhibits lower burn-in than the control $MAPbI_3$, as evidenced by the change in radiance with repeated sweeping. This may indicate that RCC3 induces a reduction in ionic motion in the emitter during electroluminescence operation.[41] In addition to enhancing stability, RCC3 incorporation also leads to a higher external quantum efficiency (EQE) over the entire current density range of testing, attributed to an increased emission intensity (Figure S11). A higher concentration of RCC3 (37 mM) leads to a lower EQE than the 5 mM device, suggesting that with higher RCC3 concentrations, the perovskite or the interfaces within the devices are likely to be excessively insulating which can negatively impact the LED stability of the device, either by requiring a large electric field for injection, joule heating at the interface, or current focusing.[42,43] Similarly, the PV parameter statistics (Table S3) show that RCC3 improves V_{OC}, especially at concentrations greater than 5 mM. Lower fill factors compromise this V_{OC} improvement due to the insulating character of RCC3 which reduces the current (Figure S12). Therefore, we limit RCC3 to 5 mM to balance the trade-off between reliability enhancement and increased series resistance. These proof-of-concept tests using partially amorphous POC-perovskite composites show that while optoelectronic performances are negatively impacted by RCC3-induced amorphization, a window of enhanced environmental stability appears at low RCC3 concentrations before the device performances

tank. Our results encourage further device optimization to break through the performance-stability trade-offs and inspire future studies on the open question regarding the potential of a fully amorphous perovskite device for energy conversion applications.

CONCLUSIONS

In this study, we incorporate POCs for the first time as functional additives to stabilize lead-halide HOIPs. Unlike smaller additives such as organic amines that increase the thin-film stability by modifying HOIP crystal structures, POC-HOIP composites, as exemplified by RCC3-$MAPbI_3$, introduce no new crystal structures but a network-like microstructure and a blue-shift in the optical bandgap. On the other hand, unlike larger additives such as polymers that increase the thin-film stability by sealing grain boundaries, as the concentration of RCC3 increases, $MAPbI_3$ grains evolve from polycrystalline to fully amorphous, where partially amorphized films significantly increase the humidity and heat resistance of $MAPbI_3$. While the general trends were reproducible across several batches, we note that the precise degradation onset changes batch-to-batch, suggesting that this RCC3-$MAPI_3$ material combination is sensitive to the processing conditions. In the best case, RCC3 was able to extend the onset of perovskite degradation by 50×, overperforming the state-of-the-art molecular engineering and capping methods under the same aging conditions. The RCC3-induced stabilization can be explained by the unique physical properties of POCs: first, the flexible framework of cage molecules enables strong hydrogen bonding between the MA^+ at the surface of $MAPbI_3$ and the -NH- moiety on the RCC3 surface. Second, the porous nature of RCC3 enables MA^+ to be trapped inside a cage via hydrogen bonding with the -NH- moiety of RCC3. We further demonstrate that the materials stabilization introduced by POCs can be translated to enhanced reliability in photovoltaic and light-emitting devices, guiding future materials and interface optimization. This work leverages the diverse chemistry of POCs and HOIPs and the combination of porous and dense materials in a single composite. We hope this will inspire further studies on molecular modifications of HOIPs for enhanced environmental stability, drawing on the burgeoning number of organic cages and macrocycles that are known.

EXPERIMENTAL SECTION

Thin film synthesis

The perovskite solution is prepared by following the established protocol. Lead (II) iodide (PbI_2) stock solution with 1.22 mol/liter nominal concentration is prepared by mixing lead (II) iodide (Sigma-Aldrich) with 9:1 *N*,*N*-dimethylformamide (Sigma-Aldrich): dimethyl sulfoxide (Sigma-Aldrich) (DMF:DMSO). For 0.1 gram of methylammonium iodide (Greatcell Solar) (MAI), 510 μL of the lead (II) iodide solution is added, resulting in $MAPbI_3$ solution with 1:1.09 molar ratio for methylammonium iodide: lead (II) iodide. Cage molecule RCC3 in powder form is then mixed with the $MAPbI_3$ solution. To make 38 mmol/liter concentration of RCC3 in $MAPbI_3$, 0.016 gram of RCC3 powder is mixed with 371 μL of $MAPbI_3$ solution. The solution can further be diluted to 20 and 5 mmol/liter. Similarly, RCC1 is mixed in a quantity of 0.011 g with 524 μL of $MAPbI_3$ perovskite solution forming a mixture of 0.025 M. The solution dissolves after significant vortexing. Then, the mixed solution is deposited on the cleaned glass slides (VWR), and spincoated in 2-step approach: 1000 rpm for 10 seconds and acceleration of 200 rpm/s, with a subsequent 6000 rpm for 30 seconds. Chlorobenzene (Sigma-Aldrich) antisolvent in the quantity of 150 μL was dropped 5 seconds at the beginning of the second step of spincoating. The films are then annealed at 100 °C for 30 minutes. We shall note due to the solubility limit variance of different batches for synthesis performed on different days, actual amount of cage molecule incorporated contain ~10% of concentration variations.

X-ray diffraction

The crystal structure of thin films is characterized using X-ray diffraction (Rigaku SmartLab), with Cu-Kα sources, and medium resolution PB/PSA mode. To measure the surface, near-surface, and bulk parts of the thin-films, the incident angles (ω) are varied: 0.08°, 0.2°, and 1°.

UV-Visible spectroscopy

The absorptance is calculated based on transmission and reflection results, which are measured using UV-Vis spectrophotometer (PerkinElmer Lambda 950) between 350-1000 nm.

Fourier-transform infrared spectroscopy

The Fourier-transform infrared spectroscopy (FTIR) for films are measured using Perkin-Elmer Spectrum 400 (Perkin-Elmer), in attenuated total reflection (ATR) configuration with ZnSe crystal. IR spectra for cage molecule powders were collected on a Bruker Tensor 27 spectrometer. Samples were analyzed as KBr disks for 16 scans with a resolution of 4 cm-1. Spectra were recorded in transmission mode.

Atomic force microscopy (AFM) / Kelvin probe force microscopy (KPFM)

AFM and KPFM images were acquired using a Veeco MultiMode 8 AFM (Bruker). Surface contact potential experiments were performed using amplitude modulated KPFM in lift mode with an applied AC voltage to the cantilever. The topography images were measured simultaneously to the KPFM images.

ASSOCIATED CONTENT

Supporting Information

Details of materials synthesis, *in situ* stability monitoring, first-principle calculations and device testing are listed in the Supporting Information.

Videos of AIMD simulations for 1) RCC3 and perovskite interface and 2) MA^+ inside RCC3 cages are included in supporting Video 1 (mapi-mai-rcc3-config-2-nvt-400K.mp4) and Video 2 (mapi-mai-rcc3-config-1-MA-in-cage-nvt-400K.mp4), respectively.

AUTHOR INFORMATION

Corresponding Author

shijings@mit.edu, Ming.Liu@liverpool.ac.uk,

aicooper@liverpool.ac.uk, buonassi@mit.edu

Present Addresses

[†]Toyota Research Institute, Los Altos, CA USA 94022

[‡]ZJU-Hangzhou Global Scientific and Technological Innovation Canter, Hangzhou 311215, China; Department of Chemistry, Zhejiang University, Hangzhou 310027, China

[§]Helmholtz-Zentrum Berlin für Materialien und Energie GmbH, Kekuléstraße 5, 12489 Berlin, Germany

Author Contributions

SS led the thin-film synthesis and characterization. ML and DH synthesized the cage molecules. JT, NTPH synthesized perovskites and performed structural, optical and degradation tests. SL led the computational calculations. YZ fabricated solar devices and performed reliability tests under the supervision of CJB. SW performed the AFM/KPFM experiments. JT fabricated light-

emitting devices and MC conducted electroluminescence and LED performance tests under supervision of VB. SS, NTPH and YW analysed the structural characterization of cage-perovskite interactions. TB, AIC and CJB discussed the results with SS and ML and provided guidance for the project. SS and TB wrote the manuscript with contributions from all authors.

Funding Sources

SS and TB acknowledge TotalEnergies SE for financial support. This study is also based upon a high-throughput imaging setup supported by the Defense Advanced Research Projects Agency (DARPA) under Contract No. HR001118C0036 (JT, NTPH, TB). YZ and CJB gratefully acknowledge the financial support through the "Aufbruch Bayern" initiative of the state of Bavaria (EnCN and "Solar Factory of the Future"), the Bavarian Initiative "Solar Technologies go Hybrid" (SolTech), "ELF-PV Design and development of solution processed functional materials for the next generations of PV technologies'' by the Bavarian State Government (No. 44-6521a/20/4) and the DFG, Projects No. 182849149 – SFB 953, IGK2495 and INST 90/1093/1. M.L and A.I.C. acknowledge the Engineering and Physical Sciences Research Council (EPSRC) (EP/N004884/1) for funding. This work was performed, in part, at the Center for Nanoscale Materials, a DOE Office of Science User Facility, and supported by the U.S. Department of Energy, Office of Science, Office of Basic Energy Sciences under Contract No. DE-AC02-06CH11357. Y.W and A.I.C. acknowledge the Leverhulme Trust via the Leverhulme Research Centre for Functional Materials Design for funding. D.H. thanks the Overseas Study Program of the Guangzhou Elite Project provided by Guangzhou City, China for financial support. SL acknowledges the use of the ARCHER2 supercomputer through membership of the UK's HPC Materials Chemistry Consortium, which is funded by EPSRC grant no. EP/R029431.

Conflicts of Interest

Although MIT PVLab has IP filed covering photovoltaic technologies and materials informatics broadly, we do not envision a direct conflict of interest with this study, the content of which is open-sourced. AIC and ML have a financial interest in the start-up company CageCapture Ltd, which is seeking to commercialize porous organic cages. TB has a financial interest in the start-up company Xinterra Pte Ltd, which applies machine learning and high-throughput experimentation to accelerate materials for sustainability.

ACKNOWLEDGMENT

SS acknowledges colleagues at MIT PVLab, Jim Serdy, and Armi Tiihonen for degradation chamber setup and software integration.

REFERENCES

(1) Boyd, C. C.; Cheacharoen, R.; Leijtens, T.; McGehee, M. D. Understanding Degradation Mechanisms and Improving Stability of Perovskite Photovoltaics. *Chemical Reviews*. American Chemical Society November 16, 2019, pp 3418–3451.

(2) Khenkin, M. V.; Katz, E. A.; Abate, A.; Bardizza, G.; Berry, J. J.; Brabec, C.; Brunetti, F.; Bulović, V.; Burlingame, Q.; Di Carlo, A.; et al. Consensus Statement for Stability Assessment and Reporting for Perovskite Photovoltaics Based on ISOS Procedures. *Nat. Energy* **2020**, *5* (1), 35–49.

(3) Liang, P.-W.; Liao, C.-Y.; Chueh, C.-C.; Zuo, F.; Williams, S. T.; Xin, X.-K.; Lin, J.; Jen, A. K.-Y. Additive Enhanced Crystallization of Solution-Processed Perovskite for Highly Efficient Planar-Heterojunction Solar Cells. *Adv. Mater.* **2014**, *26* (22), 3748–3754.

(4) Liu, S.; Guan, Y.; Sheng, Y.; Hu, Y.; Rong, Y.; Mei, A.; Han, H. A Review on Additives for Halide Perovskite Solar Cells. *Adv. Energy Mater.* **2020**, *10* (13), 1902492.

(5) Bag, S.; Durstock, M. F. Large Perovskite Grain Growth in Low-Temperature Solution-Processed Planar p-i-n Solar Cells by Sodium Addition. *ACS Appl. Mater. Interfaces* **2016**, *8* (8), 5053–5057.

(6) Choi, M. J.; Lee, Y. S.; Cho, I. H.; Kim, S. S.; Kim, D. H.; Kwon, S. N.; Na, S. I. Functional Additives for High-Performance Inverted Planar Perovskite Solar Cells with Exceeding 20% Efficiency: Selective Complexation of Organic Cations in Precursors. *Nano Energy* **2020**, *71*, 104639.

(7) Bai, S.; Da, P.; Li, C.; Wang, Z.; Yuan, Z.; Fu, F.; Kawecki, M.; Liu, X.; Sakai, N.; Wang, J. T.-W.; et al. Planar Perovskite Solar Cells with Long-Term Stability Using Ionic Liquid Additives. *Nat. 2019 5717764* **2019**, *571* (7764), 245–250.

(8) Kuang, C.; Hu, Z.; Yuan, Z.; Wen, K.; Qing, J.; Kobera, L.; Abbrent, S.; Brus, J.; Yin, C.; Wang, H.; et al. Critical Role of Additive-Induced Molecular Interaction on the Operational Stability of Perovskite Light-Emitting Diodes. *Joule* **2021**, *5* (3), 618–630.

(9) Pereyra, C.; Xie, H.; Lira-Cantu, M. Additive Engineering for Stable Halide Perovskite Solar Cells. *J. Energy Chem.* **2021**, *60*, 599–634.

(10) Chen, J.; Kim, S.-G.; Ren, X.; Jung, H. S.; Park, N.-G. Effect of Bidentate and Tridentate Additives on the Photovoltaic Performance and Stability of Perovskite Solar Cells. *J. Mater. Chem. A* **2019**, *7* (9), 4977–4987.

(11) Wu, Y.; Xie, F.; Chen, H.; Yang, X.; Su, H.; Cai, M.; Zhou, Z.; Noda, T.; Han, L. Thermally Stable MAPbI3 Perovskite Solar Cells with Efficiency of 19.19% and Area over 1 Cm2 Achieved by Additive Engineering. *Adv. Mater.* **2017**, *29* (28), 1701073.

(12) Liu, X.; Wu, J.; Guo, Q.; Yang, Y.; Luo, H.; Liu, Q.; Wang, X.; He, X.; Huang, M.; Lan, Z. Pyrrole: An Additive for Improving the Efficiency and Stability of Perovskite Solar Cells. *J. Mater. Chem. A* **2019**, *7* (19), 11764–11770.

(13) Park, C.; Ko, H.; Sin, D. H.; Song, K. C.; Cho, K. Organometal Halide Perovskite Solar Cells with Improved Thermal Stability via Grain Boundary Passivation Using a Molecular Additive. *Adv. Funct. Mater.* **2017**, *27* (42), 1703546.

(14) Zhang, F.; Zhu, K. Additive Engineering for Efficient and Stable Perovskite Solar Cells. *Adv. Energy Mater.* **2020**, *10* (13), 1902579.

(15) Yen, H. J.; Liang, P. W.; Chueh, C. C.; Yang, Z.; Jen, A. K. Y.; Wang, H. L. Large Grained Perovskite Solar Cells Derived from Single-Crystal Perovskite Powders with Enhanced Ambient Stability. *ACS Appl. Mater. Interfaces* **2016**, *8* (23), 14513–14520.

(16) Liu, Y.; Zheng, X.; Fang, Y.; Zhou, Y.; Ni, Z.; Xiao, X.; Chen, S.; Huang, J. Ligand Assisted Growth of Perovskite Single Crystals with Low Defect Density. *Nat. Commun. 2021 121* **2021**, *12* (1), 1–8.

(17) Zhu, L.; Cao, H.; Xue, C.; Zhang, H.; Qin, M.; Wang, J.; Wen, K.; Fu, Z.; Jiang, T.; Xu, L.; et al. Unveiling the Additive-Assisted Oriented Growth of Perovskite Crystallite for High Performance Light-Emitting Diodes. *Nat. Commun. 2021 121* **2021**, *12* (1), 1–8.

(18) Song, Q.; Jiang, S.; Hasell, T.; Liu, M.; Sun, S.; Cheetham, A. K.; Sivaniah, E.; Cooper, A. I. Porous Organic Cage Thin Films and Molecular-Sieving Membranes. *Adv. Mater.* **2016**, *28* (13), 2629–2637.

(19) Liu, M.; Zhang, L.; Little, M. A.; Kapil, V.; Ceriotti, M.; Yang, S.; Ding, L.; Holden, D. L.; Balderas-Xicohténcatl, R.; He, D.; et al. Barely Porous Organic Cages for Hydrogen Isotope Separation. *Science* **2019**, *366* (6465), 613–620.

(20) Liu, M.; Chen, L.; Lewis, S.; Chong, S. Y.; Little, M. A.; Hasell, T.; Aldous, I. M.; Brown, C. M.; Smith, M. W.; Morrison, C. A.; et al. Three-Dimensional Protonic Conductivity in Porous Organic Cage Solids. *Nat. Commun. 2016 71* **2016**, *7* (1), 1–9.

(21) Martínez-Ahumada, E.; He, D.; Berryman, V.; López-Olvera, A.; Hernandez, M.; Jancik, V.; Martis, V.; Vera, M. A.; Lima, E.; Parker, D. J.; et al. SO2 Capture Using Porous Organic Cages. *Angew. Chemie Int. Ed.* **2021**, *60* (32), 17556–17563.

(22) Liu, M.; Little, M. A.; Jelfs, K. E.; Jones, J. T. A.; Schmidtmann, M.; Chong, S. Y.; Hasell, T.; Cooper, A. I. Acid- and Base-Stable Porous Organic Cages: Shape Persistence and PH Stability via

Post-Synthetic "Tying" of a Flexible Amine Cage. *J. Am. Chem. Soc.* **2014**, *136* (21), 7583–7586.

(23) Xi, J.; Spanopoulos, I.; Bang, K.; Xu, J.; Dong, H.; Yang, Y.; Malliakas, C. D.; Hoffman, J. M.; Kanatzidis, M. G.; Wu, Z. Alternative Organic Spacers for More Efficient Perovskite Solar Cells Containing Ruddlesden-Popper Phases. *J. Am. Chem. Soc.* **2020**, *142* (46), 19705–19714.

(24) Liu, X.; Wang, Y.; Wu, T.; He, X.; Meng, X.; Barbaud, J.; Chen, H.; Segawa, H.; Yang, X.; Han, L. Efficient and Stable Tin Perovskite Solar Cells Enabled by Amorphous-Polycrystalline Structure. *Nat. Commun. 2020 111* **2020**, *11* (1), 1–7.

(25) Meng, Y. S.; Snaider, J.; Correa-Baena, J.-P.; Hartono, N. T. P.; Bawendi, M. G.; Holt, M. V; Li, X.; Cai, Z.; Poindexter, J. R.; Jensen, M. A.; et al. Homogenized Halides and Alkali Cation Segregation in Alloyed Organic-Inorganic Perovskites. *Science* **2019**, *363* (6427), 627–631.

(26) Viezbicke, B. D.; Patel, S.; Davis, B. E.; Birnie, D. P. Evaluation of the Tauc Method for Optical Absorption Edge Determination: ZnO Thin Films as a Model System. *Phys. status solidi* **2015**, *252* (8), 1700–1710.

(27) Rigter, S. A.; Quinn, X. L.; Kumar, R. E.; Fenning, D. P.; Massonnet, P.; Ellis, S. R.; Heeren, R. M. A.; Svane, K. L.; Walsh, A.; Garnett, E. C. Passivation Properties and Formation Mechanism of Amorphous Halide Perovskite Thin Films. *Adv. Funct. Mater.* **2021**, *31* (15), 2010330.

(28) Collavini, S.; Cabrera-Espinoza, A.; Delgado, J. L. Organic Polymers as Additives in Perovskite Solar Cells. *Macromolecules* **2021**, *54* (12), 5451–5463.

(29) Collavini, S.; Saliba, M.; Tress, W. R.; Holzhey, P. J.; Völker, S. F.; Domanski, K.; Turren-Cruz, S. H.; Ummadisingu, A.; Zakeeruddin, S. M.; Hagfeldt, A.; et al. Poly(Ethylene Glycol)–[60]Fullerene-Based Materials for Perovskite Solar Cells with Improved Moisture Resistance and Reduced Hysteresis. *ChemSusChem* **2018**, *11* (6), 1032–1039.

(30) Zhao, Y.; Wei, J.; Li, H.; Yan, Y.; Zhou, W.; Yu, D.; Zhao, Q. A Polymer Scaffold for Self-Healing Perovskite Solar Cells. *Nat. Commun.* **2016**, *7* (1), 1–9.

(31) Zhang, S. Y.; Kochovski, Z.; Lee, H. C.; Lu, Y.; Zhang, H.; Zhang, J.; Sun, J. K.; Yuan, J. Ionic Organic Cage-Encapsulating Phase-Transferable Metal Clusters. *Chem. Sci.* **2019**, *10* (5), 1450–1456.

(32) Prasanna, R.; Gold-Parker, A.; Leijtens, T.; Conings, B.; Babayigit, A.; Boyen, H. G.; Toney, M. F.; McGehee, M. D. Band Gap Tuning via Lattice Contraction and Octahedral Tilting in Perovskite Materials for Photovoltaics. *J. Am. Chem. Soc.* **2017**, *139* (32), 11117–11124.

(33) Lu, Y.; Hu, J.; Ge, Y.; Tian, B.; Zhang, Z.; Sui, M. Decisive Influence of Amorphous PbI2−x on the Photodegradation of Halide Perovskites. *J. Mater. Chem. A* **2021**, *9* (26), 15059–15067.

(34) Sun, S.; Tiihonen, A.; Oviedo, F.; Liu, Z.; Thapa, J.; Zhao, Y.; Hartono, N. T. P.; Goyal, A.; Heumueller, T.; Batali, C.; et al. A Data Fusion Approach to Optimize Compositional Stability of Halide Perovskites. *Matter* **2021**, *4* (4), 1305–1322.

(35) Jong, U.-G.; Yu, C.-J.; Ri, G.-C.; McMahon, A. P.; Harrison, N. M.; Barnes, P. R. F.; Walsh, A. Influence of Water Intercalation and Hydration on Chemical Decomposition and Ion Transport in Methylammonium Lead Halide Perovskites. *J. Mater. Chem. A* **2018**, *6* (3), 1067–1074.

(36) Hartono, N. T. P.; Thapa, J.; Tiihonen, A.; Oviedo, F.; Batali, C.; Yoo, J. J.; Liu, Z.; Li, R.; Marrón, D. F.; Bawendi, M. G.; et al. How Machine Learning Can Help Select Capping Layers to Suppress Perovskite Degradation. *Nat. Commun.* **2020**, *11* (1), 1–9.

(37) Hartono, N. T. P.; Tremblay, M. H.; Wieghold, S.; Dou, B.; Thapa, J.; Tiihonen, A.; Bulovic, V.; Nienhaus, L.; Marder, S. R.; Buonassisi, T.; et al. Tailoring Capping-Layer Composition for Improved Stability of Mixed-Halide Perovskites. *J. Mater. Chem. A* **2022**, *10* (6), 2957–2965.

(38) Mosconi, E.; Azpiroz, J. M.; De Angelis, F. Ab Initio Molecular Dynamics Simulations of Methylammonium Lead Iodide Perovskite Degradation by Water. *Chem. Mater.* **2015**, *27* (13), 4885–4892.

(39) Zheng, C.; Rubel, O. Unraveling the Water Degradation Mechanism of CH3NH3PbI3. *J. Phys. Chem. C* **2019**, *123* (32), 19385–19394.

(40) Yuan, Y. Di; Dong, J.; Liu, J.; Zhao, D.; Wu, H.; Zhou, W.; Gan, H. X.; Tong, Y. W.; Jiang, J.; Zhao, D. Porous Organic Cages as Synthetic Water Channels. *Nat. Commun. 2020 111* **2020**, *11* (1), 1–10.

(41) Zhao, L.; Gao, J.; Lin, Y. L.; Yeh, Y.-W.; Lee, K. M.; Yao, N.; Loo, Y.-L.; Rand, B. P. Electrical Stress Influences the Efficiency of CH3NH3PbI3 Perovskite Light Emitting Devices. *Adv. Mater.* **2017**, *29* (24), 1605317.

(42) Zhao, L.; Roh, K.; Kacmoli, S.; Kurdi, K. Al; Jhulki, S.; Barlow, S.; Marder, S. R.; Gmachl, C.; Rand, B. P. Thermal Management Enables Bright and Stable Perovskite Light-Emitting Diodes. *Adv. Mater.* **2020**, *32* (25), 2000752.

(43) Yoo, J. J.; Wieghold, S.; Sponseller, M. C.; Chua, M. R.; Bertram, S. N.; Hartono, N. T. P.; Tresback, J. S.; Hansen, E. C.; Correa-Baena, J.-P.; Bulović, V.; et al. An Interface Stabilized Perovskite Solar Cell with High Stabilized Efficiency and Low Voltage Loss. *Energy Environ. Sci.* **2019**, *12* (7), 2192–2199.

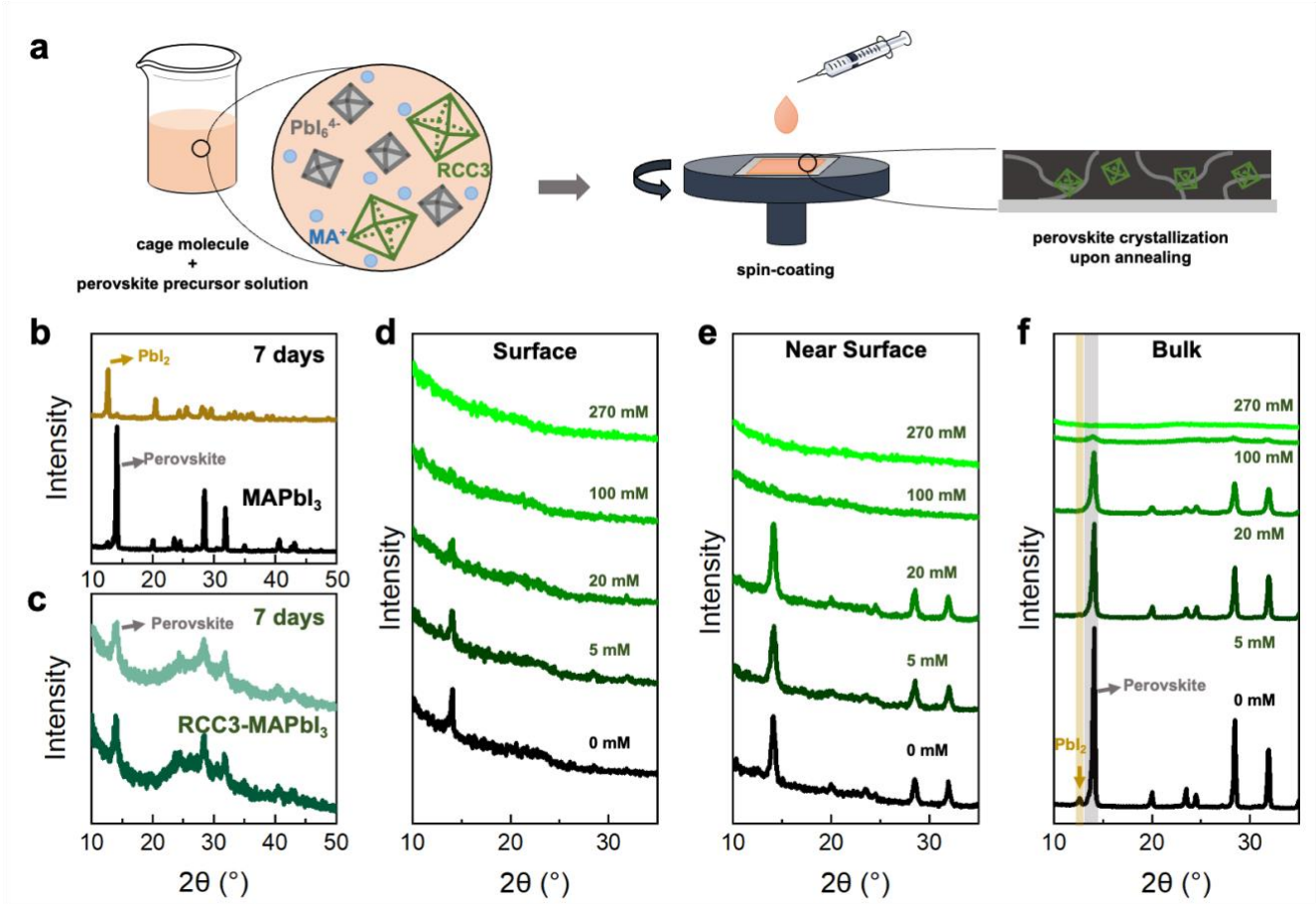

Figure 1(a) Solution synthesis workflow for POC-HOIP thin films. Grazing-incidence X-ray diffraction (GIXRD) patterns are shown for (b) as-synthesized and after-7-days $MAPbI_3$ and (c) as-synthesized and after-7-days RCC3-$MAPbI_3$ (37 ± 3 mM RCC3 in precursor solution). RCC3-$MAPbI_3$ films were examined with GIXRD incident angles of (d) 0.08°, (e) 0.2°, and (f) 1° to probe the crystal structure of films at various penetration depths.

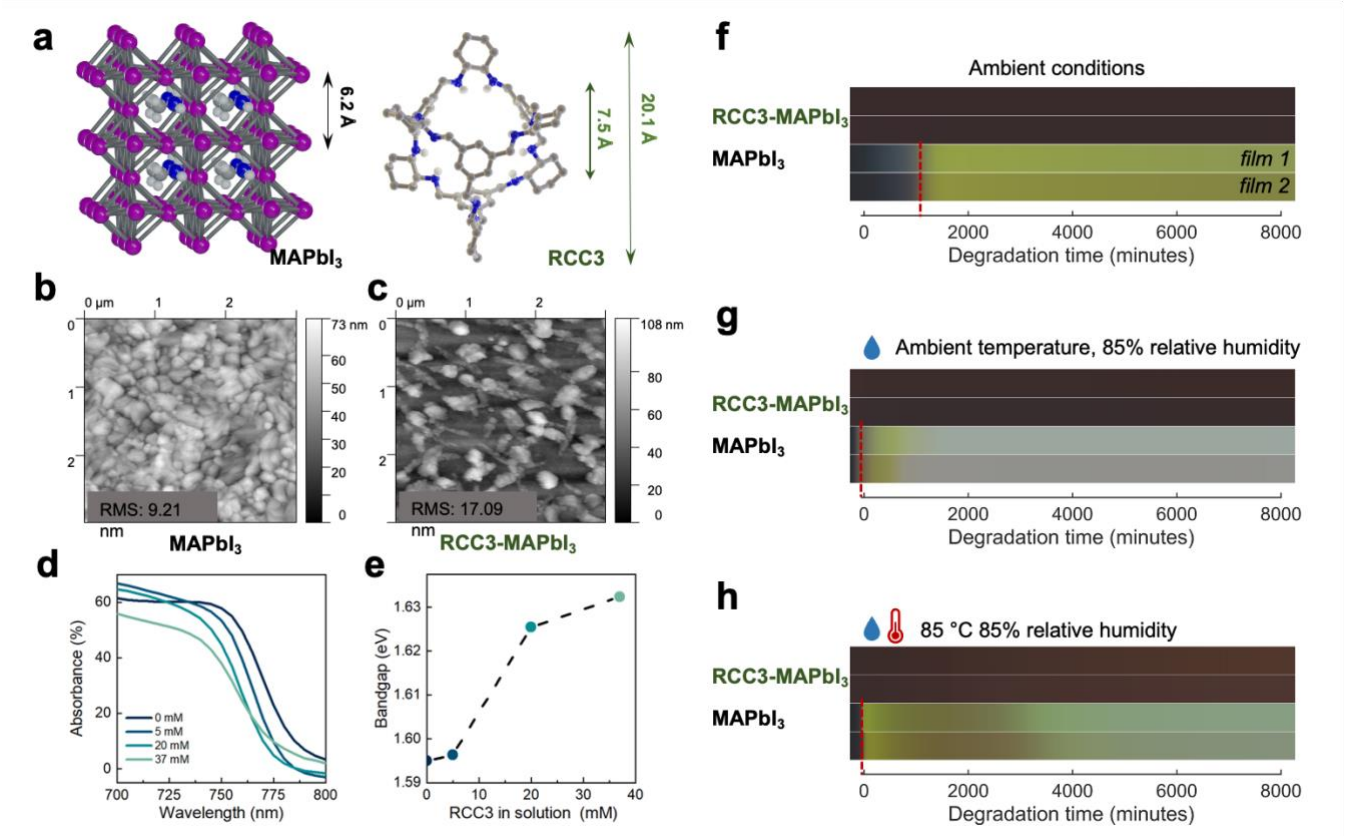

Figure 2 (a) Crystal structures of $MAPbI_3$ and RCC3. Carbon and nitrogen atoms are shown in grey and blue, respectively. Hydrogen atoms in RCC3 are omitted for clarity, except in the secondary amine group of RCC3. Atomic force microscopy (AFM) images are presented for (b) $MAPbI_3$ and (c) RCC3-$MAPbI_3$ (37 ± 3 mM RCC3 in precursor solution). RMS units are in nm. (d) Absorption edges of RCC3-$MAPbI_3$ films measured by UV-visible spectroscopy and (e) optical bandgaps of RCC3-$MAPbI_3$ estimated by the Tauc method (estimated standard deviation of 2%) as a function of POC concentration in precursor solution.[26] (f)-(h) *In situ* optical imaging of perovskite thin-film degradation under ambient conditions (October, MA, USA), 85% relative humidity (RH) at ambient temperature, and 85% RH at 85 °C, respectively (all with 0.15 Sun illumination for imaging). For each composition, two as-synthesized films of (1 × 0.5) in^2 were degraded side-by-side for repeatability purposes. RCC3 – 37 mM - $MAPbI_3$ was used for all the *in situ* film degradation tests.

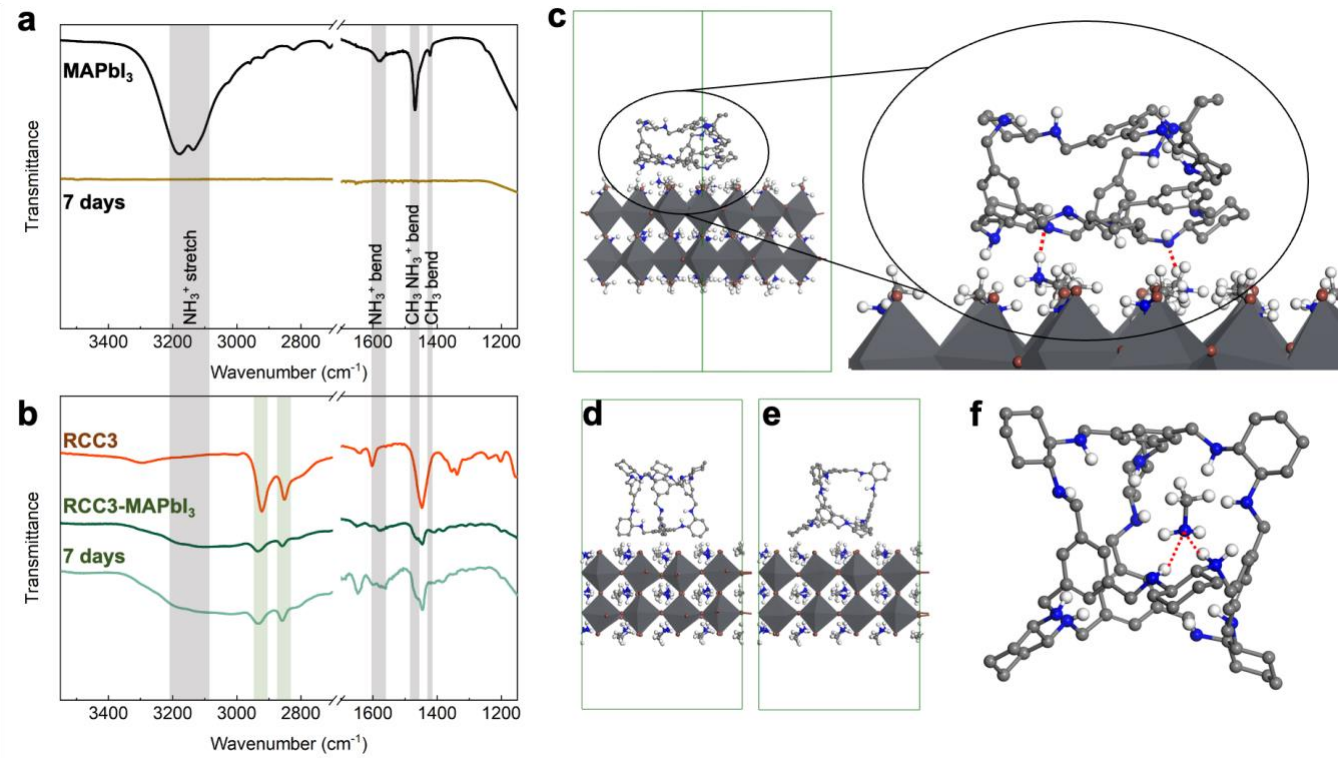

Figure 3 (a) Attenuated total reflection-Fourier transform infrared spectroscopy (ATR-FTIR) measurements for as-synthesized $MAPbI_3$ films and $MAPbI_3$ stored for seven days in ambient conditions (October, MA, USA). (b) ATR-FTIR spectra for as-synthesized RCC3 powder, as-synthesized RCC3-$MAPbI_3$ (37 ± 3 mM RCC3 in precursor solution) and RCC3-$MAPbI_3$ stored for seven days in ambient conditions same as 3 (a). Key features of an as-synthesized $MAPbI_3$ thin film and RCC3 powder are highlighted in grey and green, respectively as references. (c) DFT optimized structure of nonporous RCC3 on $MAPbI_3$ (001) surface, with initial structure taken from the AIMD trajectory. Red dotted lines indicate hydrogen bonds. Hydrogen atoms in RCC3 (except those bonded to N) are omitted for clarity. (d)-(e) DFT optimized structures of $MAPbI_3$/RCC3 interface with two different configurations: (d) config-1, benzene facet of RCC3 on $MAPbI_3$ and (e) config-2, hollow facet on $MAPbI_3$. (f) MA^+ in RCC3 with intermolecular proton transfer. Red dotted lines indicate hydrogen bonds. Hydrogen atoms in RCC3 (except those bonded to N) are omitted for clarity. Colour code: H - white, C - light grey, N - blue, O - red, Pb - dark grey, I - brown.

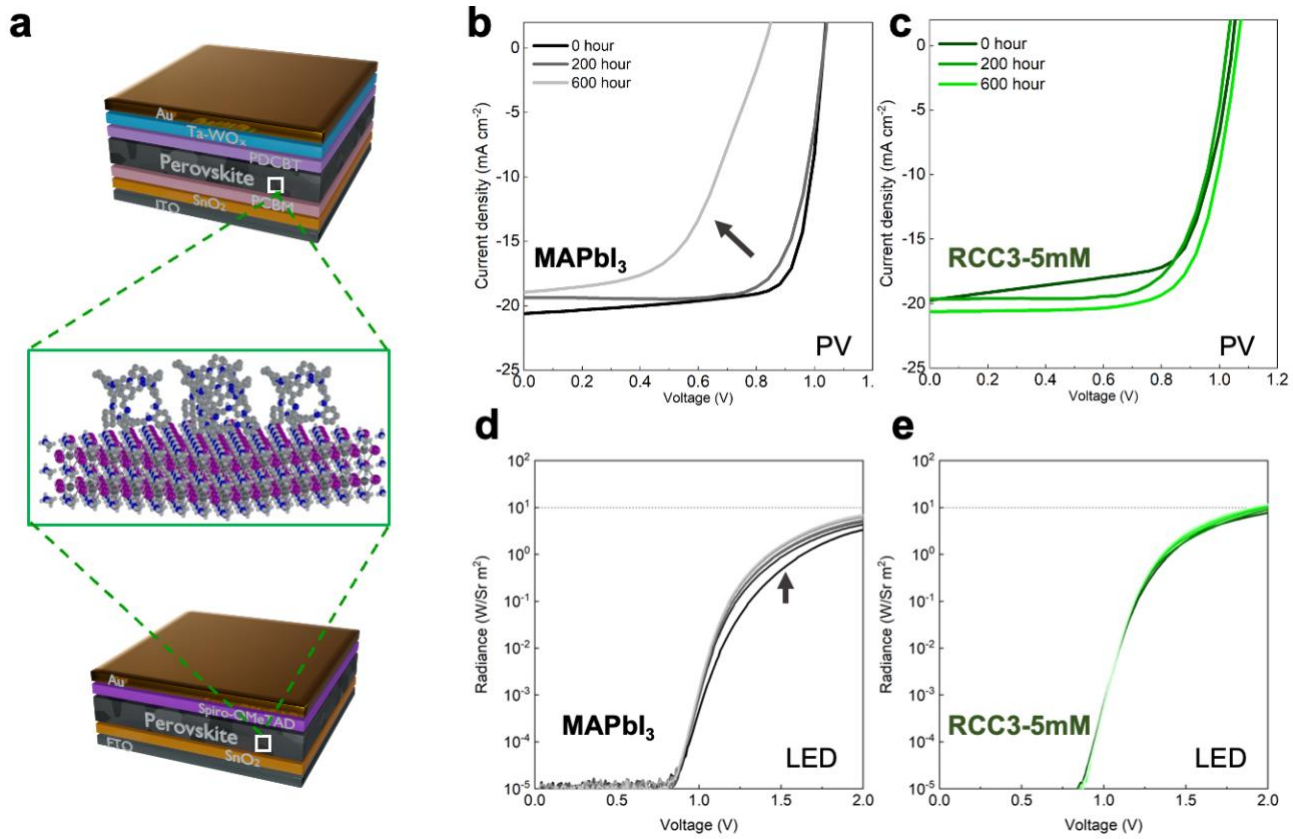

Figure 4 (a) Device architecture of solar cells and LEDs fabricated in this study. The locations shown for the cage molecules are for illustration purposes only and are not meant to indicate precise lattice locations. (b)-(c) Operation stability of solar devices based on $MAPbI_3$ and RCC3-5 mM-$MAPbI_3$, respectively. (d)-(e) Illumination of light-emitting devices based on $MAPbI_3$ and RCC3-5 mM-$MAPbI_3$ as a function of voltage sweeps.

TOC